Precision Intracellular Delivery Based on Optofluidic Polymersome Rupture

Andreas E. Vasdekis,[†,⊥] Evan A. Scott,[‡,⊥] Conlin P. O'Neil,[‡] Demetri Psaltis,[†] and Jeffrey. A. Hubbell[‡,§,*]

[†]Optics Laboratory, School of Engineering, [‡]Institute of Bioengineering, and [§]Institute of Chemical Sciences and Engineering, École Polytechnique Fédérale de Lausanne (EPFL), CH-1015 Lausanne, Switzerland. [⊥]These authors contributed equally.

ABSTRACT

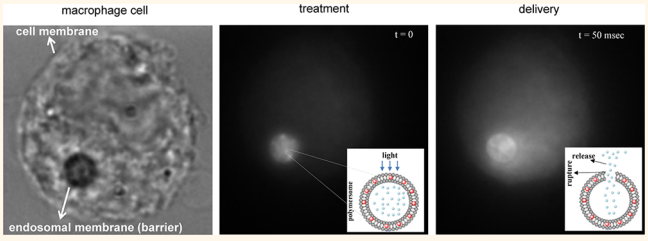

We present an optical approach for intracellular delivery of molecules contained within oxidation-sensitive polymersomes. The photosensitizer ethyl eosin is associated with the polymersome membrane to oxidatively increase the hydrophilicity of the hydrophobic block under optical excitation. This optofluidic interaction induces rapid polymersome rupture and payload release *via* the reorganization of the aggregate structure into smaller diameter vesicles and micelles. When the particles are endocytosed by phagocytes, such as RAW macrophages and dendritic cells, the polymersomes' payload escapes the endosome and is released in the cell cytosol within a few seconds of illumination. The released payload is rapidly distributed throughout the cytosol within milliseconds. The presented optofluidic method enables fast delivery and distribution throughout the cytosol of individual cells, comparable to photochemical internalization, but a factor of 100 faster than similar carrier mediated delivery methods (*e.g.*, liposomes, polymersomes, or nanoparticles). Due to the ability to simultaneously induce payload delivery and endosomal escape, this approach can find applications in detailed characterizations of intra- and intercellular processes. As an example in quantitative cell biology, a peptide antigen was delivered in dendritic cells and MHC I presentation kinetics were measured at the single cell and single complex level.

KEYWORDS: polymersomes · vesicles · immunology · biophotonics · single-cell analysis · optofluidics

Intracellular delivery has attracted substantial attention due to applications in therapy and investigations into cellular function.[1−5] The transport selectivity of the cell membrane has been circumvented by permeabilizing the cell membrane with mechanical,[6,7] electrical,[8,9] or optical means, such as photoporation[10,11] and photochemical internalization (PCI).[12−14] A less perturbative approach involves carrier-mediated strategies, such as viral vectors,[15] photosensitive caged compounds,[16] microcapsules,[17,18] and liposomal[19] or the more stable polymeric[20,21] nanoscale vesicles. Vesicle-mediated delivery has attracted substantial attention in disease therapy, due to their enhanced target specificity and capacity to encapsulate a wide range of payloads. Under the application of external stimuli, release from vesicles can be controlled and hence spatiotemporally modulate cellular function. On-demand modulation of cellular function has greatly impacted therapies and quantitative cell studies.[9,22] Typical triggers for vesicle release are ultrasound, magnetic, and optical fields.[5] Optical fields have advantages due to their enhanced spatial and temporal control and widespread use in biophotonic applications such as microscopy and optogenetics.

Here, we explore the benefits from the high stability of polymeric vesicular nanocarriers formed from self-assembling block copolymer amphiphiles (polymersomes), engineered to be sensitive to light. We demonstrate an optofluidic strategy to perturb the polymersome morphology and achieve precise intracellular delivery at the submicrometer and subsecond resolution levels. The polymersomes were formed from the oxidation-sensitive block copolymer poly(ethylene glycol)-*block*-poly(propylene sulfide) (PEG_{17}-*b*-PPS_{30})[20] (Figure 1a). Light locally activated a photosensitizer to oxidatively increase the hydrophilicity of the hydrophobic block (PPS) of the amphiphile. Polymersome stability is highly sensitive to the hydrophilic/hydrophobic balance of the constituent block copolymer, and small changes in this ratio can result in micelle instead of vesicle formation.[23] The photo-oxidation step perturbs this balance and thus destabilizes the block copolymer lamellar phase habit, leading to rupture and payload release. The optically driven modification of the surface energy of the fluid lyotropic polymersome membrane manifests the method's optofluidic character.[24,25]

Optical nanocarrier destabilization has been previously explored,[26,27] yet employing

* Address correspondence to jeffrey.hubbell@epfl.ch.

Received for review May 14, 2012 and accepted August 17, 2012.

Published online August 18, 2012
10.1021/nn302122h

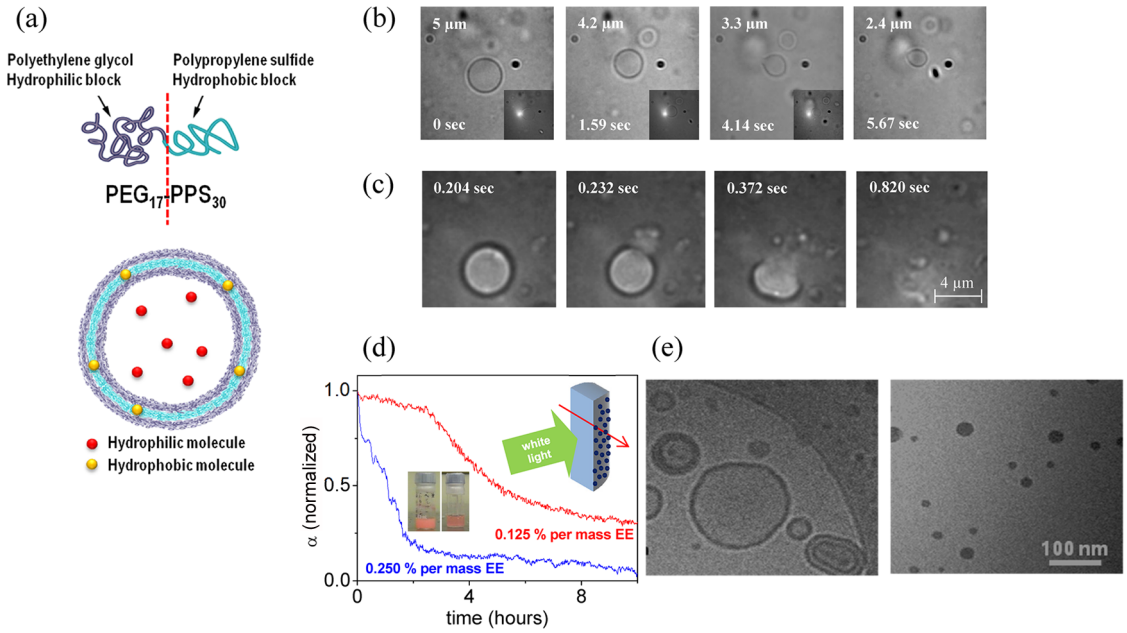

Figure 1. Concept of optofluidic polymersome rupture. (a) Chemical structure and schematic of PEG_{17}-*b*-PPS_{30} block copolymers and vesicles; PEG is the hydrophilic and PPS the hydrophobic block. (b) Localized illumination of single vesicles for 1−2 s that leads to the formation of smaller diameter vesicles; vesicle diameters are indicated in each frame, while insets show the optical treatment location at power densities of approximately 100 W/cm^2. (c) Rupture of a single polymersome in a series of video microscopy frames; illumination was at 500 W/cm^2; in subsequent optical treatments, a collimated excitation beam was employed giving rise to lower excitation densities. (d) In bulk suspensions, photo-oxidative morphology changes are manifested in decreases in turbidity, here shown in response to white light at 18 mW/cm^2. Variations in the sensitizer concentration are manifested as different release profiles; insets show a schematic of the experimental setup and two colored photographs of the sensitized suspension before (left) and after illumination (right). (e) Cryogenic transmission electron microscopy images confirm the transition from vesicles to spherical micelles after photo-oxidation.

damaging short wavelength radiation[28] or causing relatively weak and slow membrane perturbations; such slow destabilization kinetics effectively limit the temporal resolution in quantifying kinetics of cellular processes.[29−31] Rapid payload delivery and cytosolic distribution has been demonstrated with PCI-based methods, with temporal resolution in the subsecond levels.[13] On the contrary, light-driven intracellular delivery based on carrier-mediated delivery such as vesicles and capsules[17,32,33] or metallic nanoparticles[34,35] has so far been limited to a temporal resolution of several minutes. One carrier-mediated approach achieved cellular response in approximately 10 s after optical triggering of nanoscale liposomes; however, prior to optical triggering, the nanocarriers needed 2−3 h to first escape the endosome.[36] Although typically slower, nanocarrier-based delivery systems present several advantages in comparison to PCI. In PCI, photo-oxidizers and bioactive molecules are delivered separately, and differences in cellular uptake can hinder colocalization within the same endosomal compartment prior to illumination.[37] In a nanocarrier-based system, photo-oxidizers and bioactive molecules are retained within the same nanoparticle to ensure both protection from as well as colocalization within the endosomal environment. The optofluidic method discussed here combines the encapsulation capacity of carrier-based delivery with the speed of PCI since, under short illuminations, payload distribution throughout the cytosol takes place within approximately 50 ms. We attribute these rapid kinetics of endosomal escape to the unique capability of polymersomes to convert into micellar surfactants capable of introducing pores into endosomal membranes at sufficiently high concentrations.[38] For optical treatment, visible radiation was employed, which can be extended to the near-infrared by choosing alternative photosensitizers with high one or two photon absorption cross sections at these wavelengths.

RESULTS AND DISCUSSION

The polymersomes were photosensitized through the incorporation of ethyl eosin. This hydrophobic dye readily associates with the PPS-rich inner leaflet of the membrane with 93% encapsulation efficiency (Supplementary Figure 1). To directly visualize the effect of the illumination, we imaged micrometer-scale vesicles suspended in water and irradiated with a 488 nm laser beam. In Figure 1b, such a measurement is illustrated, where polymersomes received a 1−2 s treatment, focused on a small area of the membrane with a 600 nm spot. The small excitation area gave rise to excitation densities of approximately 100 W/cm^2. This treatment gave rise to localized destabilization of the polymersome membrane and the formation of smaller diameter vesicles. Illumination of the whole

polymersome for longer periods resulted in a complete destabilization of the polymersomes (Figure 1c).

We observed an interesting behavior when the photosensitized polymersomes were subjected to long-term illumination with a collimated incoherent light beam. As shown in Figure 1d, the suspension turbidity decreases under illumination, indicating that the average particle size also decreases. After approximately 10 h of illumination, the average particle size decreased from 245 nm down to 60 nm as determined by dynamic light scattering measurements. This particle size change suggests a transition from vesicles to micelles. The formation of micelles is likely due to the increased hydrophilicity of the hydrophobic block and thermodynamically driven reorganization of the aggregate structure. Micelle formation was confirmed by cryogenic transmission electron microscopy (Figure 1e). The possibility to employ white incoherent light can potentially enable targeted delivery using cost-effective light sources (*e.g.*, lamps). Such sources could be deployed in illuminating cell cultures at broad excitation areas. Sensitizers at different concentrations or with different spectral responses can be co-encapsulated in the polymersomes to control the temporal profile of the release under white-light excitation conditions (Figure 1d).

Photosensitized oxidation can involve a number of different pathways.[39] To explore the underlying mechanism, turbidity measurements were performed in the presence of either the oxygen scavenger hydrazine or the singlet oxygen ($^1O_2$) quencher NaN_3.[40] The strong inhibition of morphology change in the presence of hydrazine or NaN_3, respectively, verifies the presence of an oxygen-dependent reaction and indicates that $^1O_2$ generation is the dominant mechanism (Figure 2a and inset). Wavelengths not efficiently absorbed by ethyl eosin did not cause any morphological changes. This was determined by DLS, which indicated that the average particle diameter decreased from approximately 150 to 54 nm by employing wavelengths within the ethyl eosin absorption spectrum (inset of Figure 2a). To investigate the exact mechanism of the polymersome rupture, NMR spectroscopy was performed on illuminated samples (see Methods). The NMR measurement indicated that, upon illumination, the hydrophobic PPS block is converted to a more hydrophilic poly(propylene sulfoxide) derivative (Figure 2b). The conversion percentage was approximately 20% (Figure 2b and Supporting Information). Gel permeation chromatography (GPC) revealed only a slight increase in polydispersity of the PEG_{17}-*b*-PPS_{30}, indicating minimal chain cleavage induced by photo-oxidation (Supplementary Figure 2).

The kinetics of polymersome rupture and release were explored using a single-particle assay (see Methods). At the single-particle level, detailed rupture kinetics can be revealed (Figure 1c), contrary to bulk

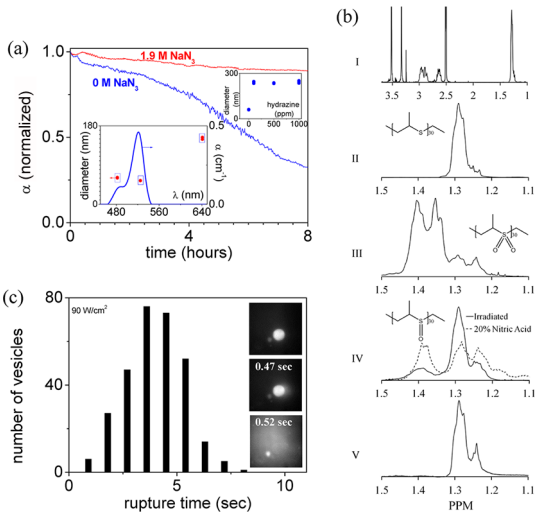

Figure 2. Origins of polymersome morphological changes under optical excitation. (a) Polymersome photo-oxidation is inhibited in the presence of the $^1O_2$ quencher NaN_3, here manifested by time-dependent turbidity variations under optical excitation; the bottom inset plots the average particle diameter (red spheres) dependence on the excitation wavelength as determined by dynamic light scattering and of the absorption spectrum of ethyl eosin (blue line); top inset plots the particle diameter as measured by DLS of particle suspensions that received the same amount of illumination but at different hydrazine concentrations. (b) ^1H NMR spectra of PEG_{17}-*b*-PPS_{30} before (I,II) and after (III−IV) oxidation. The shift in protons within the CH_3 groups of the PPS block after photo-oxidation was compared to selective oxidation of the PPS block to sulfones and sulfoxides: CH_3 protons before oxidation (II), after reaction with 10% hydrogen peroxide (III), after reaction with 20% nitric acid (IV, dotted line), and after photo-oxidation with ethyl eosin at 488 nm excitation for 10 h (IV, solid line) and after illumination of calcein-loaded polymersomes without ethyl eosin at 488 nm excitation for 10h (V). (c) Single-particle studies reveal the time required for rupture and calcein release from photosensitive polymersomes under optical excitation (n = 300 observations). A typical measurement is shown in the inset with a series of fluorescent images of a single polymersome (1.6 μm in diameter) releasing its payload.

studies performed in suspensions where rupture kinetics can be masked by the propagation of the photo-oxidizing radiation through the turbid medium. Ethyl eosin was co-encapsulated with calcein at a self-quenching concentration (30 mM). This allowed the monitoring of payload release *via* the evolution of the fluorescent signal due to calcein dequenching (Figure 2c). Subsequent to rupture, calcein is released in an explosive burst, approximately 8 times faster than passive diffusion. This transport mechanism is attributed to the higher osmotic pressure within the polymersome than the surrounding, due to its higher concentration of membrane-impermeable calcein and salt (PBS 50 mM) and possibly elevated localized temperatures during optical excitation or production of reactive oxygen species.[41] For a polymersome formulation similar to what was subsequently employed in intracellular delivery, approximately 75% of the polymersomes required less than 4.5 s of irradiation to release (Figure 2c). Calcein may also contribute to

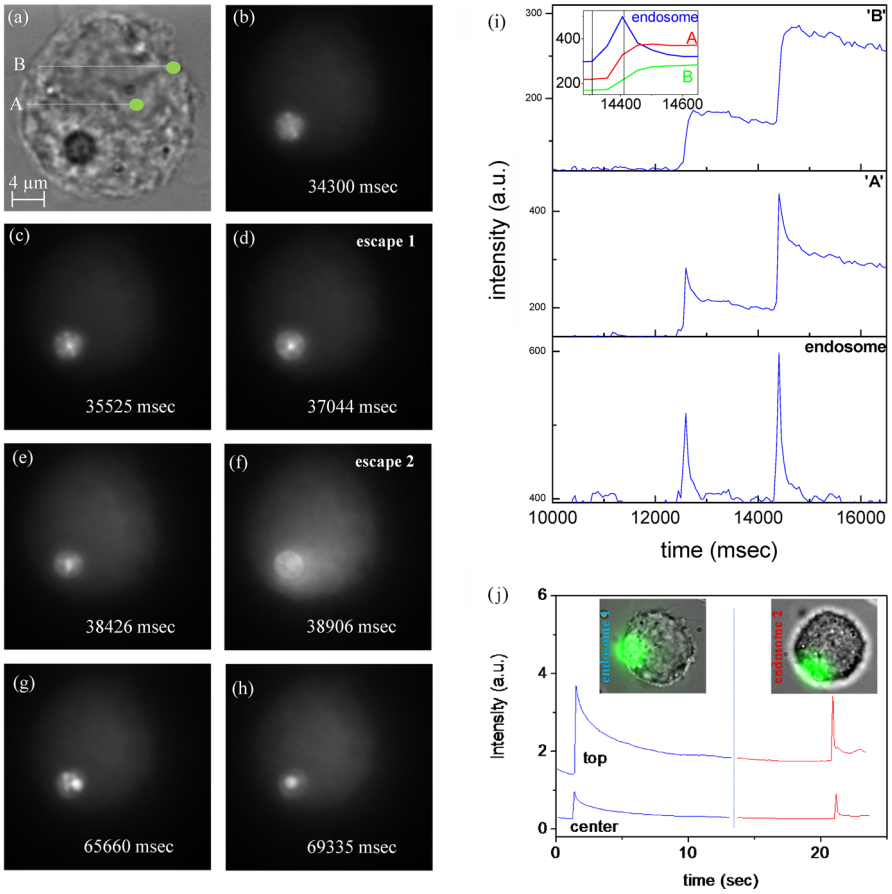

Figure 3. Endosomal escape with optofluidic polymersome rupture in macrophages. (a–h) Series of fluorescent microscopy frames show polymersomes that have been taken up by RAW macrophage cells rupturing under optical excitation, releasing their contents in the endosome and cytosol; endosomal escape is illustrated in panels (d) and (f). (i) Optically triggered release of calcein is mapped by the fluorescent intensity variation inside the endosome and cytosol. "A" and "B" specify the locations where calcein release was imaged by measuring the time-dependent fluorescence; inset is a magnified view of the previous graphs showing that release first takes place in the endosome and then the cytosol (*y*-axis is scaled for visualization). (k) Intensity variation at two different locations in a single cell (center and top) due to the release from two individual endosomes at different time points; the inset shows the location and release from the two endosomes.

the polymersome morphology change due to its photo-oxidation properties.[42] However, we found that calcein was not as efficient as ethyl eosin, demonstrating slower release kinetics by more than a factor of 2 (Supplementary Figure 3). Due to its water solubility, calcein is not retained within the polymersome membrane for a localized reaction with short-lived singlet oxygen species. Under the same 10 h illumination conditions, polymersomes loaded solely with calcein were not found by NMR to be significantly oxidized (Figure 2b). When neither ethyl eosin nor calcein was encapsulated within the polymersomes, no rupture was observed under illumination during the single-vesicle levels or bulk studies.

Intracellular delivery was explored in RAW macrophage cells, chosen for their high rate of endocytosis and ability to phagocytose large particles, allowing high spatial resolution imaging (Figure 3a and Supplementary video 1). The cells were incubated for 2 h with polymersomes loaded with both ethyl eosin (to induce rupture) and calcein (to visualize rupture). Under the conditions of 2 h incubation, the polymersomes were found always intact within the endosomes prior to optically triggered cytosolic delivery. This suggests that there was inadequate time for fusion of endosomes with lysosomes to take place that would effectively lead to polymersome degradation. Under no illumination, no release from the polymersomes or endosomes was detectable after 2 h, as also previously observed under similar conditions.[43] During exposure to a 488 nm beam, endosomal spatiotemporal intensity variations initially take place (Figure 3b–d). These intensity variations are likely due to vesicle fusion inside the endosome (Figure 3g,h); the leakage level during this process depends on the distance between the vesicles that undergo fusion (Supplementary Figure 4). A typical fusion of polymersomes within an endosome can be observed in Figure 3g,h, where two separate vesicles fuse to form a single larger one (see also Supplementary video 2). These light-driven intra-endosomal processes were not found to be extensively leaky (Supplementary Figure 4). During single-particle

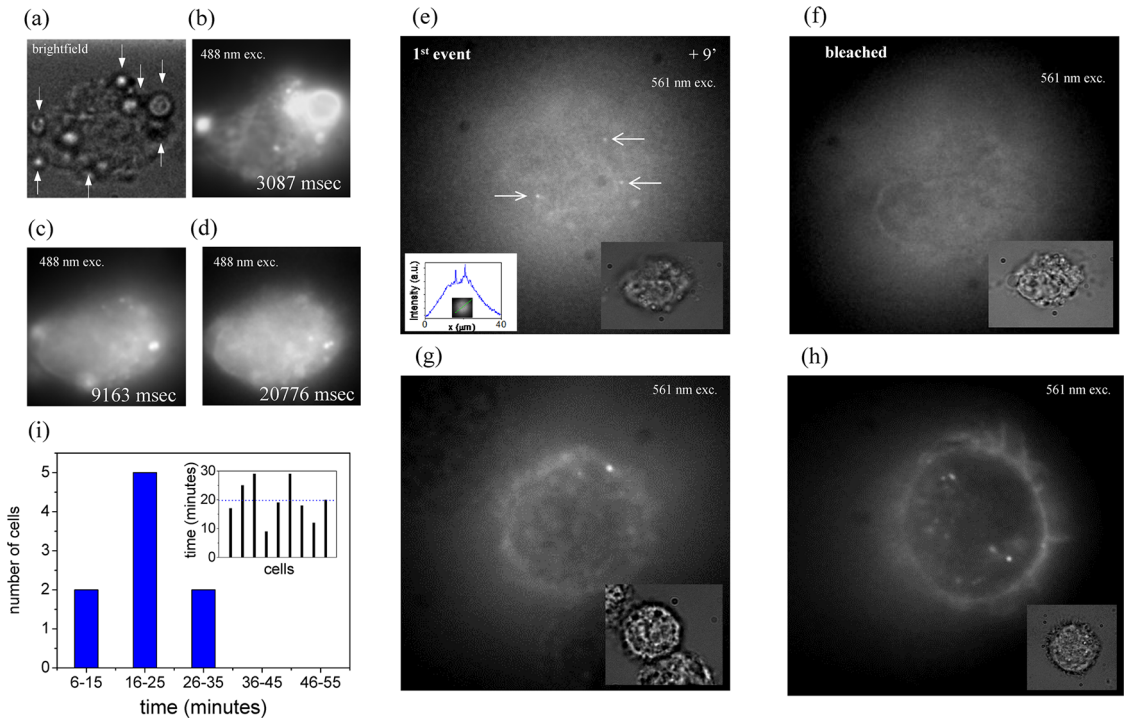

Figure 4. Antigen presentation in dendritic cells. (a–d) Optofluidic polymersome rupture can enable the release of the MHC I binding peptide SIINFEKL, shown here in the series of fluorescent images. (e) Presentation events on the cell membrane are manifested as localized fluorescent spots, shown with arrows on a cell at a time point of 9 min after release. (f) After bleaching the spots in (e), the same cell did not exhibit a similar signal in subsequent recordings. Similar presentation levels and events were observed in cases where SIINFEKL was delivered *via* a 2 h (g) or overnight (h) incubation. Not all cells exhibit the same presentation kinetics due to their inherent cell heterogeneity, as manifested in the plot of the time points of the first antigen presentation event for nine different dendritic cells (i); the histogram indicates that the majority of events take place between 16 and 25 min.

studies without cells, polymersomes that were confined within a bigger block copolymer vesicle (vesosomes) were observed to undergo fusion under illumination when in close proximity to each other (Supplementary Figure 4c).

Vesicle rupture and payload release were manifested as strong fluorescence increases in the endosome and subsequently across the cytosol (Figure 3d,f). The fluorescence intensity inside the endosome decreases to background levels within approximately 400 ms after payload release, indicating that endosomal escape is both rapid and complete (Figure 3i). Endosomal escape is attributed to the PPS block associating with and temporarily permeabilizing the endosomal membrane as independently observed in passive release experiments (Supplementary Figure 5).[44] The observation of multiple release events indicates that endosomes reseal and remain intact.[13,45] The high speed of the endosomal escape is attributed to the osmotic swelling of the endosome with respect to the cytosol resulting from accumulation of reactive oxygen species and released calcein, as well as to localized temperature increases due to light absorption.[41] Typically, the first endosomal release occurs within the first 15 s of illumination. The calcein payload was imaged as it spread from cytosol location A to location B (Figure 3a). The payload distribution throughout the cytosol required approximately 50 ms after endosomal escape. Illumination of cells either with or without endocytosed ethyl eosin- and calcein-loaded polymersomes at similar excitation conditions was found to have no effect on cell viability for up to 2 min of exposure (Supplementary Figure 6). While similar optical treatment duration has been reported using polymeric microcapsules,[46] the almost instantaneous delivery throughout the cell cytosol is similar to PCI and, to our knowledge, of the fastest reported based on optical nanocarrier destabilization.[17,32–36] By focusing the same excitation field into an approximately 600 nm diameter area, it was possible to address single endosomes in individual cells. Triggered cytosolic delivery from single endosomes was achieved in this way, opening thus the possibility for both time and space multiplexed cytosolic release (Figure 3j); the differences in the two transport profiles are attributed to the stochastic nature of phagocytosis, which introduces variability in endosome size and content.

To demonstrate the precise spatial and temporal control afforded by this method, we explored the loading of peptide antigens from the cytosol onto the major histocompatibility complex I (MHC I) of dendritic cells (DCs).[1] The timing of this process is critical for immune processes including cancer immunotherapy[47] and due to lack of available methods has not been

well-characterized. Polymersomes were loaded with the octapeptide ovalbumin MHC I epitope SIINFEKL (100 μM), along with ethyl eosin and calcein. Bone-marrow-derived murine dendritic cells were incubated for 2 h to allow endosomal uptake of polymersomes (Figure 4a). Endosomal escape was induced within individual cells by the aforementioned optofluidic treatment. This allowed us to record the time of the peptide release into the cytosol with millisecond precision (Figure 4b–d and Supplementary video 3). Endosomal escape within the DCs required treatment of approximately 6 s (Supplementary Figure 7). Antigen presentation was visualized with a fluorescently tagged antibody specific for the SIINFEKL peptide loaded in the MHC I complex. Antibody binding on the cell membrane was detected as individual fluorescent spots at a different excitation wavelength (561 nm) than the one used for release (Figure 4e). On average, the duration for the first presentation event was 19.8 $\pm$ 6.9 min (Figure 4i; mean $\pm$ SD), and for more than 50% of the cells studied, a second presentation event took place at a later time. Recent measurements of the intracellular diffusion coefficient of short peptides indicate that within the measured duration of antigen presentation the peptide can travel across the cell approximately 200 times.[48] This value suggests that the peptide's passive diffusion is not likely to be the rate-limiting step in antigen presentation, in agreement with the current consensus that presentation kinetics are limited by the high probability of peptide degradation before reaching the endoplasmic reticulum.[49] We observed similar presentation events occurring after a 2 h incubation of the cells with unencapsulated SIINFEKL (Figure 4g) with presentation being stronger in the case of overnight incubation (Figure 4h). No antigen presentation was observed when no SIINFEKL was delivered, either passively *via* vesicle degradation or actively *via* optofluidic polymersome rupture. While previous works[8,17,50,51] have primarily focused on characterizing antigen presentation in population studies either by measuring the cytotoxic T cell responses, flow cytometry, or imaging at the single-cell level, the optofluidic delivery presented here enabled the direct measurement with high precision of the kinetics of this biochemical pathway at the single-cell and even single-peptide MHC I complex level.

CONCLUSION

In conclusion, we demonstrated an optofluidic method that permits precisely controlled polymersome rupture for intracellular delivery. Contrary to conventional delivery methods, the proposed optofluidic approach enables both high spatial precision and almost instantaneous endosomal escape of the polymersome payload without damaging cellular membranes. With this method, we delivered antigens to DCs and precisely measured the kinetics of antigen loading upon MHC I. We anticipate this optofluidic technique will enable novel applications in controlling cellular activity relevant to the characterization of cellular processes, as well as in therapeutics for studies on both single and populations of cells. The localized and low level of photo-oxidation required for triggered release can be generated with standard white lamps or even sunlight, allowing broad applicability with standard laboratory equipment. While phagocytic cells were utilized in the current study, the versatility of block copolymer chemistry allows adaptation of this method for targeting the endocytic pathways of almost any cell type. Cells containing recently phagocytized polymersomes were also observed to release their payload toward their extracellular environment (Supplementary Figure 8), suggesting still other applications.

METHODS

Block Copolymer Synthesis Characterization. Unless otherwise stated, all chemicals were purchased from Sigma. PEG_{17}-*b*-PPS_{30} (M_n of 2700, PEG weight fraction of 0.28) was synthesized as previously described;[23] briefly, the living polymerization of propylene sulfide was initiated with benzyl mercaptan and capped with mesylate-functionalized PEG methyl ether (Supplementary Figure 9). The product was precipitated in methanol, and purity was verified by gel permeation chromatography (GPC) using Waters Styragel THF columns (HR 2, 3, and 4) with a tetrahydrofuran (THF) mobile phase *via* both refractive index and UV/vis detectors (Waters Corporation). ^{1}H NMR in DMSO-d_6: δ = 1.26–1.32 (m, CH_3, PPS), 2.58–2.69 (m, CH, PPS), 2.82–3.01 (m, CH_2, PPS), 3.24–3.26 (OCH_3, PEG), 3.49–3.54 (CH_2, PEG), 7.16–7.19 (d, CH_{aromat}).

To identify the degree of oxidation of the irradiated polymersomes, polymersomes (3.7 mM) were reacted in aqueous solutions of either 10% hydrogen peroxide, which is expected to produce a mixture of sulfoxide and sulfones,[52] or 10% nitric acid, which has been shown to selectively oxidize PPS to poly(propylene sulfoxide).[53] Samples were lyophilized prior to ^{1}H NMR analysis. ^{1}H NMR in DMSO-d_6 after oxidation with hydrogen peroxide: δ = 1.26–1.32 (m, CH_3, PPS), 1.33–1.38 (m, CH_3, polypropylene sulfone), 1.38–1.46 (m, CH_3, polypropylene sulfone), 2.82–3.01 (m, CH_2, PPS), 3.24–3.26 (OCH_3, PEG), 3.49–3.54 (CH_2, PEG), 7.16–7.19 (d, CH_{aromat}). ^{1}H NMR in DMSO-d_6 after oxidation with nitric acid: δ = 1.26–1.32 (m, CH_3, PPS), 1.33–1.45 (m, CH_3, polypropylene sulfoxide), 2.58–2.69 (m, CH, PPS), 2.82–3.01 (m, CH_2, PPS), 3.24–3.26 (OCH_3, PEG), 3.49–3.54 (CH_2, PEG), 7.16–7.19 (d, CH_{aromat}). Polymersomes irradiated in the presence of ethyl eosin displayed identical NMR spectra as samples reacted with nitric acid (Figure 2b).

Polymersome Preparation and Characterization. Polymersomes were formed by either solvent dispersion or thin film rehydration. The polydispersity index of the polymer was 1.12 (Supplementary Figure 2). For both methods, ethyl eosin was first separately dissolved in a 90% ethanol solution at 7 mM, and the diblock/ethyl eosin molar ratio during polymersome formation was 106:1. During solvent dispersion, PEG_{17}-*b*-PPS_{30} (20 mM) was dissolved in THF with or without the addition of ethyl eosin and added dropwise to water at a 0.025:1:5 (ethanol/THF/water) ratio followed by desiccation to remove the THF. Unloaded ethyl eosin, ethanol, and residual THF were removed by dialysis.

Thin film rehydration was performed by dissolving PEG_{17}-*b*-PPS_{30} in dichloromethane with or without the addition of ethyl eosin and then desiccating the solution for 2 h to form thin films. Films were rehydrated by overnight rotation at 4 °C in 50 mM PBS containing either or both calcein (30 mM) or SIINFEKL

(100 μM). Loaded polymersomes were purified from unloaded molecules first by dialysis (MWCO 10 kDa, Thermo Scientific, Rockford, IL) and subsequently by size exclusion chromatography with a Sepharose CL-6B column. Purification was verified with UV/fluorescence HPLC (Waters Alliance 2695, Waters Corporation).

Polymersomes were characterized with dynamic light scattering (DLS) and cryogenic electron microscopy (cryo-TEM). DLS analysis was performed with polymersome suspensions in PBS (1 mL, 0.1 mg/mL) using a Zetasizer Nano ZS (Malvern Instruments,). For cryo-TEM, polymersome suspensions in PBS (5 μL at 1 mg/mL) were applied to carbon-coated copper grids (400 mesh, Agar Scientific) and plunged into liquid ethane (−127 °C) to prepare films of vitreous ice using the bare-grid technique.[54] Grids were placed in a Gatan cryoholder and analyzed at −180 °C with a Philips/FEI CM12 transmission electron microscope at a voltage of 100 kV. Images were recorded with a Gatan 794 slow scan digital camera.

Turbidity Assay. The bulk particle rupture experiments were performed in a cuvette at concentrations of approximately 0.75 mg/mL, unless otherwise stated. Illumination for rupture was provided with a white-light source (X-Cite 120Q, Lumen Dynamics) at specified powers and an excitation area of approximately 2 cm^2. Band-pass color filters (Shemrock) were placed in front of the white-light beam path in order to select certain excitation wavelengths. Transmission was measured with a He−Ne laser (Newport Corporation) or an infrared diode laser and was detected by a sensitive CCD camera (Apogee Imaging Systems, US).

Single-Particle Assay. The single-particle and cell experiments were performed on an inverted frame microscope (IX71, Olympus, Japan), equipped with a high-resolution stage (MS-2000, Applied Scientific Instrumentation, OR, USA) and a 100×, NA = 1.45 objective (PLAPO100XO/TRIFM-SP, Olympus, Japan). Images and videos were captured with an EMCCD camera (iXon DV885 VP, Andor Technology, Ireland) cooled to −80 °C. The time resolution of the measurements was in most cases approximately 20 ms, while the spatial resolution was 200 nm, as determined by single-molecule fluorescent measurements. For these experiments, vesicle rupture was induced with the 488 nm line of an argon ion laser (Innova 300, Coherent, US).

Optofluidic Intracellular Delivery. Microfluidic chambers (300 μm thickness and 1 cm wide) were fabricated *via* cast molding lithography. Briefly, SU-8 photoresist (Gersteltec Inc., Switzerland) was spun on a Si wafer and patterned with contact-mode optical lithography. The structured SU-8 was treated with trimethylchlorosilane vapor for 2 min (Sigma Aldrich), and the pattern was subsequently transferred to PDMS (Dow Corning) at a ratio of monomer−catalyst ratio at 10:1 *via* cast-molding. The structured PDMS was placed in an O_2 plasma chamber (15 W, 20 s) to permanently bond to a similarly treated glass coverslip. The glass coverslips received a cleaning protocol as previously described.[55] The bonded microchannels were additionally cleaned with 2 M NaOH and coated with sterile 0.01% aqueous solutions of poly-L-lysine.

RAW 264.7 macrophages or bone-marrow-derived dendritic cells were seeded at 100 000 cells/mL in 12-well tissue culture plates (Falcon) and incubated with 0.5 mg/mL polymersome solutions in DMEM for 2 h at 37 °C. After washing with DMEM, cells were scraped off the surface of the wells and injected into the microfluidics chambers. Within the chambers, adhered cells were preincubated for 30 min with 2.4G2 FcR-blocking antibody (Invitrogen) in DMEM. Immediately prior to imaging, a phycoerythin-tagged 25-D1.16 SIINFEKL/MHC I-specific antibody solution (10 μg/mL, eBiosciences) in DMEM containing the 2.4G2 FcR-blocking antibody was flowed over the surface of the cells.

Cell treatment was performed in the same setup employed in the single-particle assay, with power densities of approximately 50−80 mW/cm^2, unless otherwise stated. For imaging, a solid-state laser operating at 561 nm was employed (Newport Corporation, US). The SIINFEKL peptide loaded in the MHC I complex was visualized on the cell membrane as individual localized fluorescent spots. These bright spots appeared at subsequent time points after the optofluidic release; prolonged illuminations at 561 nm led to their disappearance over time due to bleaching. The obtained fluorescent images were correlated with bright-field images of the cell to ensure that these spots were not due to "lensing" effects due to the three-dimensional cell morphology.

Conflict of Interest: The authors declare no competing financial interest.

Acknowledgment. This work was supported by the Whitaker Foundation, the Bill and Melinda Gates Foundation, and the European Research Council grant NanoImmune.

Supporting Information Available: Supplementary figures are available, as cited throughout the text, namely, the gel permeation chromatography of the polymersomes before and after illumination, rupture kinetics of vesicles loaded only with calcein, polymersome fusion, passive release from polymersomes (*i.e.*, no irradiation), polymersome payload release within BMDCs and in the extracellular environment, and finally the synthesis of PEG_{17}-*b*-PPS_{30} and subsequent oxidation by reactive oxygen species. Two supplementary videos are included, illustrating intracellular delivery within macrophage cells (Supplementary video 1), endosomal polymersome fusion (Supplementary video 2), and within BMDCs (Supplementary video 3). This material is available free of charge *via* the Internet at http://pubs.acs.org.

REFERENCES AND NOTES

1. Hubbell, J. A.; Thomas, S. N.; Swartz, M. A. Materials Engineering for Immunomodulation. *Nature* **2009**, *462*, 449–460.
2. Luo, D.; Saltzman, W. M. Synthetic DNA Delivery Systems. *Nat. Biotechnol.* **2000**, *18*, 33–37.
3. Pack, D. W.; Hoffman, A. S.; Pun, S.; Stayton, P. S. Design and Development of Polymers for Gene Delivery. *Nat. Rev. Drug Discovery* **2005**, *4*, 581–593.
4. Peer, D.; Karp, J. M.; Hong, S.; FaroKhzad, O. C.; Margalit, R.; Langer, R. Nanocarriers as an Emerging Platform for Cancer Therapy. *Nat. Nanotechnol.* **2007**, *2*, 751–760.
5. Prokop, A. *Intracellular Delivery Fundamentals and Applications*; Springer: Berlin, 2011.
6. Okada, C. Y.; Rechsteiner, M. Introduction of Macromolecules into Cultured Mammalian-Cells by Osmotic Lysis of Pinocytic Vesicles. *Cell* **1982**, *29*, 33–41.
7. O'Brien, J. A.; Lummis, S. C. R. Biolistic Transfection of Neuronal Cultures Using a Hand-Held Gene Gun. *Nat. Protoc.* **2006**, *1*, 977–981.
8. Harding, C. V. Electroporation of Exogenous Antigen into the Cytosol for Antigen Processing and Class I Major Histocompatibility Complex (MHC) Presentation: Weak Base Amines and Hypothermia (18°C) Inhibit the Class I MHC Processing Pathway. *Eur. J. Immunol.* **1992**, *22*, 1865–1869.
9. Boukany, P. E.; Morss, A.; Liao, W.-C.; Henslee, B.; Jung, H.; Zhang, X.; Yu, B.; Wang, B.; Wu, Y.; Li, L.; *et al.* Nanochannel Electroporation Delivers Precise Amounts of Biomolecules into Living Cells. *Nat. Nanotechnol.* **2011**, *6*, 747–754.
10. Tirlapur, U. K.; Konig, K. Cell Biology - Targeted Transfection by Femtosecond Laser. *Nature* **2002**, *418*, 290–291.
11. Paterson, L.; Agate, B.; Comrie, M.; Ferguson, R.; Lake, T. K.; Morris, J. E.; Carruthers, A. E.; Brown, C. T. A.; Sibbett, W.; Bryant, P. E.; *et al.* Photoporation and Cell Transfection Using a Violet Diode Laser. *Opt. Express* **2005**, *13*, 595–600.
12. Berg, K.; Folini, M.; Prasmickaite, L.; Selbo, P. K.; Bonsted, A.; Engesaeter, B. O.; Zaffaroni, N.; Weyergang, A.; Dietze, A.; Maelandsmo, G. M.; *et al.* Photochemical Internalization: A New Tool for Drug Delivery. *Curr. Pharm. Biotechnol.* **2007**, *8*, 362–372.
13. de Bruin, K. G.; Fella, C.; Ogris, M.; Wagner, E.; Ruthardt, N.; Brauchle, C. Dynamics of Photoinduced Endosomal Release of Polyplexes. *J. Controlled Release* **2008**, *130*, 175–182.
14. Berg, K.; Selbo, P. K.; Prasmickaite, L.; Tjelle, T. E.; Sandvig, K.; Moan, D.; Gaudernack, G.; Fodstad, O.; Kjolsrud, S.; Anholt, H.; *et al.* Photochemical Internalization: A Novel Technology for Delivery of Macromolecules into Cytosol. *Cancer Res.* **1999**, *59*, 1180–1183.

15. Nayak, S.; Herzog, R. W. Progress and Prospects: Immune Responses to Viral Vectors. *Gene Ther.* **2010**, *17*, 295–304.
16. Adams, S. R.; Tsien, R. Y. Controlling Cell Chemistry with Caged Compounds. *Annu. Rev. Physiol.* **1993**, *55*, 755–784.
17. Palankar, R.; Skirtach, A. G.; Kreft, O.; Bedard, M.; Garstka, M.; Gould, K.; Mohwald, H.; Sukhorukov, G. B.; Winterhalter, M.; Springer, S. Controlled Intracellular Release of Peptides from Microcapsules Enhances Antigen Presentation on MHC Class I Molecules. *Small* **2009**, *5*, 2168–2176.
18. Javier, A. M.; del Pino, P.; Bedard, M. F.; Ho, D.; Skirtach, A. G.; Sukhorukov, G. B.; Plank, C.; Parak, W. J. Photoactivated Release of Cargo from the Cavity of Polyelectrolyte Capsules to the Cytosol of Cells. *Langmuir* **2008**, *24*, 12517–12520.
19. Hope, M. J.; Bally, M. B.; Webb, G.; Cullis, P. R. Production of Large Unilamellar Vesicles by a Rapid Extrusion Procedure - Characterization of Size Distribution, Trapped Volume and Ability To Maintain a Membrane Potential. *Biochim. Biophys. Acta, Bioenerg.* **1985**, *812*, 55–65.
20. Napoli, A.; Valentini, M.; Tirelli, N.; Muller, M.; Hubbell, J. A. Oxidation-Responsive Polymeric Vesicles. *Nat. Mater.* **2004**, *3*, 183–189.
21. Discher, D. E.; Eisenberg, A. Polymer Vesicles. *Science* **2002**, *297*, 967–973.
22. Spiller, D. G.; Wood, C. D.; Rand, D. A.; White, M. R. H. Measurement of Single-Cell Dynamics. *Nature* **2010**, *465*, 736–745.
23. Cerritelli, S.; O'Neil, C. P.; Velluto, D.; Fontana, A.; Adrian, M.; Dubochet, J.; Hubbell, J. A. Aggregation Behavior of Poly(ethylene glycol-*bl*-propylene sulfide) Di- and Triblock Copolymers in Aqueous Solution. *Langmuir* **2009**, *25*, 11328–11335.
24. Psaltis, D.; Quake, S. R.; Yang, C. H. Developing Optofluidic Technology through the Fusion of Microfluidics and Optics. *Nature* **2006**, *442*, 381–386.
25. Monat, C.; Domachuk, P.; Eggleton, B. J. Integrated Optofluidics: A New River of Light. *Nat. Photonics* **2007**, *1*, 106–114.
26. Alvarez-Lorenzo, C.; Bromberg, L.; Concheiro, A. Light-Sensitive Intelligent Drug Delivery Systems. *Photochem. Photobiol.* **2009**, *85*, 848–860.
27. Timko, B. P.; Dvir, T.; Kohane, D. S. Remotely Triggerable Drug Delivery Systems. *Adv. Mater.* **2010**, *22*, 4925–4943.
28. Mabrouk, E.; Cuvelier, D.; Brochard-Wyart, F.; Nassoy, P.; Li, M. H. Bursting of Sensitive Polymersomes Induced by Curling. *Proc. Natl. Acad. Sci. U.S.A.* **2009**, *106*, 7294–7298.
29. Anderson, V. C.; Thompson, D. H. Triggered Release of Hydrophilic Agents from Plasmalogen Liposomes Using Visible Light or Acid. *Biochim. Biophys. Acta, Bioenerg.* **1992**, *1109*, 33–42.
30. De Geest, B. G.; McShane, M. J.; Demeester, J.; De Smedt, S. C.; Hennink, W. E. Microcapsules Ejecting Nanosized Species into the Environment. *J. Am. Chem. Soc.* **2008**, *130*, 14480–14482.
31. Robbins, G. P.; Jimbo, M.; Swift, J.; Therien, M. J.; Hammer, D. A.; Dmochowski, I. J. Photoinitiated Destruction of Composite Porphyrin-Protein Polymersomes. *J. Am. Chem. Soc.* **2009**, *131*, 3872–3874.
32. Miller, C. R.; Clapp, P. J.; O'Brien, D. F. Visible Light-Induced Destabilization of Endocytosed Liposomes. *FEBS Lett.* **2000**, *467*, 52–56.
33. Yavlovich, A.; Singh, A.; Blumenthal, R.; Puri, A. A Novel Class of Photo-Triggerable Liposomes Containing DPPC: DC(8,9)PC as Vehicles for Delivery of Doxorubcin to Cells. *Biochim. Biophys. Acta, Biomembr.* **2011**, *1808*, 117–126.
34. Lee, S. E.; Liu, G. L.; Kim, F.; Lee, L. P. Remote Optical Switch for Localized and Selective Control of Gene Interference. *Nano Lett.* **2009**, *9*, 562–570.
35. Huschka, R.; Neumann, O.; Barhoumi, A.; Halas, N. J. Visualizing Light-Triggered Release of Molecules Inside Living Cells. *Nano Lett.* **2010**, *10*, 4117–4122.
36. Gregersen, K. A. D.; Hill, Z. B.; Gadd, J. C.; Fujimoto, B. S.; Maly, D. J.; Chiu, D. T. Intracellular Delivery of Bioactive Molecules Using Light-Addressable Nanocapsules. *ACS Nano* **2010**, *4*, 7603–7611.
37. Norum, O.-J.; Selbo, P. K.; Weyergang, A.; Giercksky, K.-E.; Berg, K. Photochemical Internalization (PCI) in Cancer Therapy: From Bench towards Bedside Medicine. *J. Photochem. Photobiol., B* **2009**, *96*, 83–92.
38. Christian, D. A.; Cai, S.; Bowen, D. M.; Kim, Y.; Pajerowski, J. D.; Discher, D. E. Polymersome Carriers: From Self-Assembly to siRNA and Protein Therapeutics. *Eur. J. Pharm. Biopharm.* **2009**, *71*, 463–474.
39. Foote, C. S. Mechanisms of Photosensitized Oxidation. *Science* **1968**, *162*, 963–970.
40. Valenzeno, D. P. Photomodification of Biological Membranes with Emphasis on Singlet Oxygen Mechanisms. *Photochem. Photobiol.* **1987**, *46*, 147–160.
41. Zhu, T. F.; Szostak, J. W. Exploding Vesicles. *J. Syst. Chem.* **2011**, *2*, 1–6.
42. Beghetto, C.; Renken, C.; Eriksson, O.; Jori, G.; Bernardi, P.; Ricchelli, F. Implications of the Generation of Reactive Oxygen Species by Photoactivated Calcein for Mitochondrial Studies. *Eur. J. Biochem.* **2000**, *267*, 5585–5592.
43. Cerritelli, S.; Velluto, D.; Hubbell, J. A. PEG-SS-PPS: Reduction-Sensitive Disulfide Block Copolymer Vesicles for Intracellular Drug Delivery. *Biomacromolecules* **2007**, *8*, 1966–1972.
44. Yuba, E.; Kojima, C.; Harada, A.; Tana; Watarai, S.; Kono, K. pH-Sensitive Fusogenic Polymer-Modified Liposomes as a Carrier of Antigenic Proteins for Activation of Cellular Immunity. *Biomaterials* **2010**, *31*, 943–951.
45. Neil, A. E.; Madler, L.; Velegol, D.; Xia, T.; Hoelk, E. M. V.; Somasundaran, P.; Klaessig, F.; Castranova, V.; Thompson, M. Understanding Biophysicochemical Interactions at the Nano-Bio Interface. *Nat. Mater.* **2009**, *8*, 543–557.
46. Skirtach, A. G.; Javier, A. M.; Kreft, O.; Kohler, K.; Alberola, A. P.; Mohwald, H.; Parak, W. J.; Sukhorukov, G. B. Laser-Induced Release of Encapsulated Materials Inside Living Cells. *Angew. Chem., Int. Ed.* **2006**, *45*, 4612–4617.
47. Cho, N.-H.; Cheong, T.-C.; Min, J.-H.; Wu, J.-H.; Lee, S.-J.; Kim, D.; Yang, J.-S.; Kim, S.; Kim, Y.-K.; Seong, S.-Y. A Multifunctional Core−Shell Nanoparticle for Dendritic Cell-Based Cancer Immunotherapy. *Nat. Nanotechnol.* **2011**, *6*, 675–682.
48. Reits, E.; Griekspoor, A.; Neijssen, J.; Groothuis, T.; Jalink, K.; van Veelen, P.; Janssen, H.; Calafat, J.; Drijfhout, J. W.; Neefjes, J. Peptide Diffusion, Protection, and Degradation in Nuclear and Cytoplasmic Compartments Before Antigen Presentation by MHC Class I. *Immunity* **2003**, *18*, 97–108.
49. Yewdell, J. W. Not Such a Dismal Science: The Economics of Protein Synthesis, Folding, Degradation and Antigen Processing. *Trends Cell Biol.* **2001**, *11*, 294–297.
50. Kukutsch, N. A.; Rossner, S.; Austyn, J. M.; Schuler, G.; Lutz, M. B. Formation and Kinetics of MHC Class I-Ovalbumin Peptide Complexes on Immature and Mature Murine Dendritic Cells. *J. Invest. Dermatol.* **2000**, *115*, 449–453.
51. Kim, D. T.; Mitchell, D. J.; Brockstedt, D. G.; Fong, L.; Nolan, G. P.; Fathman, C. G.; Engleman, E. G.; Rothbard, J. B. Introduction of Soluble Proteins into the MHC Class I Pathway by Conjugation to an HIV Tat Peptide. *J. Immunol.* **1997**, *159*, 1666–1668.
52. Napoli, A.; Tirelli, N.; Kilcher, G.; Hubbell, J. A. New Synthetic Methodologies for Amphiphilic Multiblock Copolymers of Ethylene Glycol and Propylene Sulfide. *Macromolecules* **2001**, *34*, 8913–8917.
53. Oyama, T.; Naka, K.; Chujo, Y. Polymer Homologue of DMSO: Synthesis of Poly(ethylene sulfoxide) by Selective Oxidation of Poly(ethylene sulfide). *Macromolecules* **1999**, *32*, 5240–5242.
54. Dubochet, J.; Adrian, M.; Chang, J. J.; Homo, J. C.; Lepault, J.; Mcdowall, A. W.; Schultz, P. Cryo-Electron Microscopy of Vitrified Specimens. *Q. Rev. Biophys.* **1988**, *21*, 129–228.
55. Cuennet, J.; Vasdekis, A. E.; De Sio, L.; Psaltis, D. Optofluidic Modulator Based on Peristaltic Nematogen Microflows. *Nat. Photonics* **2011**, *5*, 234–238.